

Barium Ferrites Loaded TiO₂ Usage In Photocatalytic Degradation of Rhodamine B Under Visible Light

Görünür Işık Altında Rodamin B'nin Fotokatalitik Parçalanmasında Baryum Ferrit Yüklenmiş TiO₂ Kullanılması

Research Article

Özge Kerkez Kuyumcu

Chemical Engineering Department, Faculty of Engineering, Marmara University, İstanbul, Turkey.

ABSTRACT

In the present study, the barium ferrites sample was synthesized by conventional citrate method as a first step, then it was used with different amounts in TiO₂ synthesis via a soft hydrolysis method as a second step. Resulted photocatalyst samples were named as BaFts/TiO₂. The samples were characterized by X-ray diffraction (XRD), UV-vis diffuse reflectance spectra (DRS) and scanning electron microscopy (SEM). The samples were tested in Rhodamine B degradation under visible light. Rhodamine B degradation efficiency was increased approximately 2.8 times with respect to the efficiency of the naked TiO₂.

Key Words

Barium ferrite, titanium dioxide, photocatalysis, dye degradation.

ÖZ

Bu çalışmada ilk basamakta baryum ferrit örneği klasik sitrat yöntemiyle sentezlenmiştir. İkinci basamakta bu örnek hidroliz yöntemi ile TiO₂ sentezinde farklı miktarlarda kullanılmıştır. Elde edilen fotokatalizör örnekleri BaFts/TiO₂ olarak adlandırılmıştır. Örnekler X-ışını difraksiyonu (XRD), UV-görünür alan difüz reflektansı (UV-vis DRS) ve taramalı elektron mikroskobu (SEM) ile karakterize edilmiştir. Örnekler, görünür ışık altında Rodamin B parçalanmasında kullanılmıştır. Rodamin B'nin parçalanma etkinliği, yalın TiO₂'in etkinliğine kıyasla yaklaşık 2.8 kat artmıştır.

Anahtar Kelimeler

Baryum ferrit, titanyum dioksit, fotokataliz, boya parçalanması.

Article History: Received: Apr 22, 2017; Revised: Jun 25, 2017; Accepted: Oct 27, 2017; Available Online: Dec 25, 2017.

DOI: 10.15671/HJBC.2018.179

Correspondence to: Ö.K. Kuyumcu, Chemical Engineering Dep., Faculty of Engineering, Marmara University, İstanbul, Turkey.

Tel: +90 216 348 02 92 / 1517

Fax: +90 216 348 02 93

E-Mail: ozge.kuyumcu@marmara.edu.tr

INTRODUCTION

The presence of organic dyes in wastewaters is undesirable in terms of both aesthetics and human health. Organic dyes discharged to the nature with wastewaters, are hazardous for the ecosystem because of their non-biodegradability and toxicity. Numerous methods have been reported for the wastewater treatment. These physical, chemical and biological methods have disadvantages [1,2]. Heterogeneous photocatalysis, which occurs as an important part of the advanced oxidation process, is an efficient method for the wastewater treatment. Redox reactions start with the photogenerated electron-hole pair on the semiconductor photocatalyst surface by absorbing the energy required. TiO_2 is the most suitable photocatalyst because of its inertness, stability and high oxidative ability [3,4]. But TiO_2 has a disadvantage of nonfunctionality beyond the 400 nm wavelength; it can be activated only by UV irradiation because of its wide band gap. So the studies have been focused on sensitizing TiO_2 to the visible light by several types of dopants for usage with sunlight [5].

Generally noble metals (Ag, Au, Pt) or transition metals (V, Cr, Mn, Co) doped TiO_2 have been synthesized for different photocatalytic reactions [6-8]. Another way is synthesizing TiO_2 as a coupled semiconductor with a narrow band gap material such as CdS, WO_3 [9,10]. Recently, ferrites have had great attraction for the various photocatalytic processes because of their relatively narrow band gap [11]. Also, the precursor is abundant so the cost of the photocatalyst can be lowered by usage of the ferrites. If they occupy a sufficient amount in the photocatalyst, the magnetic properties facilitate the separation from the reaction media.

ZnFe_2O_4 , CuFe_2O_4 , NiFe_2O_4 , MnFe_2O_4 and CoFe_2O_4 have been widely used in photocatalytic processes [12-20]. Not only ferrites have been used singly, but also ferrites have been used as composites. For example, very recently ZnFe_2O_4 multi-porous microbricks/graphene hybrid photocatalyst was used for photocatalytic degradation of p-chlorophenol under visible light irradiation ($\lambda > 420$ nm) [21]. In a similar study, photocatalytic degradation of methylene blue was performed with $\text{ZnFe}_2\text{O}_4/\text{ZnO}$ nanocomposites immobilized

on graphene [22]. Furthermore Ca^{2+} , Mg^{2+} and Ba^{2+} cations have been used in MFe_2O_4 structure [11,23]. Photocatalytic degradation of rhodamine B was studied with $\text{MgFe}_2\text{O}_4/\text{TiO}_2$ composite prepared by milling and calcining [24]. The present metal cation in the lattice affects the stability and redox properties of the ferrites. So the different ferrites can show different photocatalytic activities according to the consisting metal, synthesis route and the other characteristic properties.

Barium ferrite is the least used ferrite compound in photocatalytic processes; there are limited studies with it. BaFe_2O_4 was used in photocatalytic degradation of methyl orange under UV light [25], BaFe_2O_4 core/silica/ TiO_2 shell was used in the photodegradation of Procion red MX-5B dye under UV illumination [26]. Very recently, $\text{BaFe}_{12}\text{O}_{19}$ (band gap 1.77 eV) was used in the photocatalytic methylene blue degradation under visible light irradiation with H_2O_2 [27]. Barium ferrite is a highly stable, inert material that is advantageous for photodegradation reactions [28].

Rhodamine B (RB) is a toxic dye that is used in textile industry. It should be eliminated from the wastewater because of the hazardous effects on the human beings and animals.

All this knowledge was led to investigate the activity of barium ferrites/ TiO_2 under visible light for photocatalytic degradation of RB. In this study barium ferrites were synthesized by citrate method, then TiO_2 was prepared in the presence of various amounts of barium ferrites. The photocatalysts were tested in terms of barium ferrites ratio in the total photocatalysts, initial RB concentration, catalyst amount and pH.

MATERIALS and METHODS

Materials

All reagents used in the experiments were used without further purification. $\text{BaCl}_2 \cdot 2\text{H}_2\text{O}$ (Merck), $\text{Fe}(\text{NO}_3)_3 \cdot 9\text{H}_2\text{O}$ (Merck), citric acid $\text{C}_6\text{H}_8\text{O}_7$ (Merck), 25% NH_3 solution (Merck), titanium isopropoxide 97% $\text{Ti}[\text{OCH}(\text{CH}_3)_2]_4$ (Aldrich), Triethanolamine (TEA) $\text{C}_6\text{H}_{15}\text{NO}_3$ (Merck), 1-propanol $\text{C}_3\text{H}_7\text{OH}$ (Merck), acetic acid CH_3COOH (Merck) were used in the synthesis of the photocatalysts.

Synthesis of Photocatalysts

Barium ferrite was prepared according to citrate method published previously [11]. The aqueous solution of $\text{Fe}(\text{NO}_3)_3 \cdot 9\text{H}_2\text{O}$ and $\text{BaCl}_2 \cdot 2\text{H}_2\text{O}$ was prepared in molar ratio of $\text{Fe}^{3+}:\text{Ba}^{2+} = 2:1$. The concentration of Ba^{2+} ion in the solution was 0.25 M. The mixture was magnetically stirred for 30 min. 3 g of $\text{C}_6\text{H}_8\text{O}_7$ was added and the mixture was stirred at 60°C , approximately 6 ml of ammonia solution was added by dropwise until its pH value became 6-7. After stirring 8 h, the gel was dried at 120°C and calcined at 900°C for 1 h.

BaFts/ TiO_2 samples were prepared by a soft hydrolysis method. Dispersion of BaFts was prepared under ultrasound in glacial acetic acid as 0.066 g/mL. Separately, a mixture of $\text{Ti}[\text{OCH}(\text{CH}_3)_2]_4$ and TEA was prepared in 1-propanol. A specified amount of BaFts dispersion was added to this mixture to obtain various w/w ratios of BaFts/photocatalyst (0.5%, 1.0%, 2.5%, 5.0%). The mixture was kept under ultrasound for 30 min and H_2O was added to achieve the hydrolysis reaction for the synthesis of TiO_2 . And then 10 mL 1-propanol was added to dilute. The final volume of the mixture was 30 mL. The molar ratio of $\text{Ti}:\text{TEA}:\text{H}_2\text{O}$ was 1:1:2. The final concentration of Ti^{4+} in the mixture was 0.5 M. The mixture was kept at 70°C for overnight and at 100°C for 2 h. Finally the as-prepared gel was calcined at 500°C for 1 h. BaFts/ TiO_2 samples did not show the magnetic separation because of the low loading amount of ferrites.

Characterization

The photocatalyst samples were characterized by powder X-ray diffractions (XRD) using Rigaku D/Max-2200 diffractometer with $\text{CuK}\alpha$ ($\lambda = 1.5405$) radiation. Samples were scanned from 20° to 85° at a rate of $2^\circ/\text{min}$ (in 2θ). The diffuse reflectance spectra (DRS) of the samples in the wavelength range 200-800 nm were obtained by Ocean Optics UV-vis scanning spectrophotometer using BaSO_4 as reference. The morphological characteristics of the samples and backscattered electron analysis were carried out by Field Emission Scanning Electron Microscopy (FE-SEM, FEI Quanta FEG 450).

Photocatalytic Reactions

Photocatalytic reactions were performed with a

100 ml total volume of aqueous Rhodamine B solution with specific initial concentrations. The solution was taken to a 10 cm diameter reaction vessel placed in a reaction chamber. At the top of the reaction chamber the light source (Horoz, HL 88105105W DAYLIGHT, main emission wavelength is 530 nm) was mounted, the distance between the surface of RB solution and the lamp was 20 cm. A particular amount of photocatalyst (0.5 - 2.0 g/L) added and then the mixture was kept in the dark under stirring for 2 hours to reach the adsorption equilibrium. Before the light switching, a zero time sample was taken to determine the dye concentration after the adsorption. The temperature of the reaction mixture was kept constant at $25 \pm 2^\circ\text{C}$. Reaction aliquots were taken periodically from reaction media and filtered. RB concentration was followed by PG Instruments UV-Vis spectrophotometer at 555 nm. Degradation efficiencies were calculated by Equation 1 where C_{dye_t} = dye concentration at time t, C_{dye_0} = dye concentration at time 0.

$$\text{Degradation efficiency (\%)} = \frac{(C_{\text{dye}_0} - C_{\text{dye}_t})}{C_{\text{dye}_0}} \times 100 \quad (1)$$

RESULTS and DISCUSSION

Characterization Results

Figure 1a represents the XRD pattern of prepared barium ferrites by the citrate method. The as-prepared sample showed three phases from ferrite family. The dominant phase is $\text{BaFe}_{12}\text{O}_{19}$ which is identified by card no 00-007-0276. The diffraction peaks at 30.3° , 32.1° , 34.1° , 37.1° , 40.4° , 55° and 56.6° correspond to the planes of 110, 107, 200, 203, 205, 217 and 2011 of barium hexaferrite phase structure, respectively. BaFe_2O_4 phase is identified by the most severe two peaks of pattern with card no 01-073-3906. The diffraction peaks at 28.7° and 32.7° correspond to the planes of 221 and 061 of barium monoferrite phase structure. Finally, $\alpha\text{-Fe}_2\text{O}_3$ is characterized by the peaks at 35.2° and 40.8° which correspond to the planes of 110 and 113 of hematite structure with card no 00-033-0664 [29].

Figure 1b shows the XRD pattern of BaFts/ TiO_2 photocatalysts prepared with different amounts of the dopant. The characteristic peaks of $\text{BaFe}_{12}\text{O}_{19}$ or

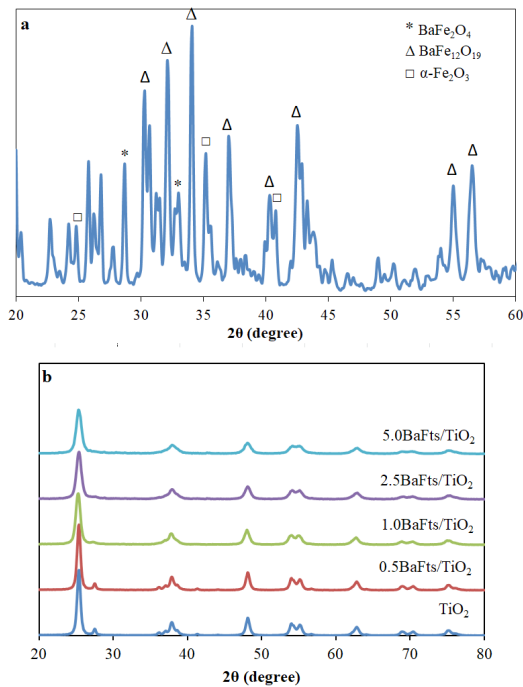


Figure 1. XRD pattern of barium ferrites synthesized by citrate method (a); XRD pattern of the BaFts/TiO₂ photocatalysts (b).

any other ferrite phase did not observe at the XRD pattern of none of the doped photocatalysts. It is attributed to low concentration of ferrites phase in the structure. However, there is an effect that can not be ignored, the intensity of the peaks which belongs to TiO₂ anatase phase decreased as the dopant amount increases. The diffraction patterns of all BaFts/TiO₂ photocatalyst samples showed the characteristic peaks of anatase phase of TiO₂ determined by JCPDS card no. 21-1272. As shown in Figure 1b, the diffraction peaks at 25.5°, 37.9°,

48.3°, and 62.9° correspond to the crystal planes of 1 0 1, 0 0 4, 2 0 0, and 2 0 4 of TiO₂ anatase phase structure.

The crystallite sizes were calculated by Scherrer equation given in Equation 2 where k is a constant between 0.8 and 1.39, λ is the wavelength of the X-rays, β is the full width at half maximum, θ is the Bragg angle, and D is the crystallite size (Å).

$$D_{hkl} = \frac{k \cdot \lambda}{\beta \cdot \cos \theta} \quad (2)$$

The mean crystallite sizes, given in Table 1, were calculated as using the maximum intensity peak with $I/I_0 = 100$. The mean crystallite sizes of the BaFts/TiO₂ photocatalysts are lower than naked TiO₂ and barium ferrite structure. It was realized that the presence of BaFts during TiO₂ formation resulted lower crystallite size of doped photocatalysts. Even, when the amount of BaFts was increased from 0.5 to 1.0 the mean crystallite size was decreased from 14.3 nm to 12.8 nm. For the higher amounts of BaFts, no more reduction was observed in crystallite size; which indicated there is a limiting level in terms of BaFts amount for crystallite size reduction of doped photocatalysts.

Figure 2a represents the UV-vis absorption spectra of the photocatalysts. As expected, the naked TiO₂ showed the minimum visible light absorbance. The naked BaFts showed quite excess absorbance in visible light. Coupling of TiO₂ with BaFts enhanced the absorption in the visible light

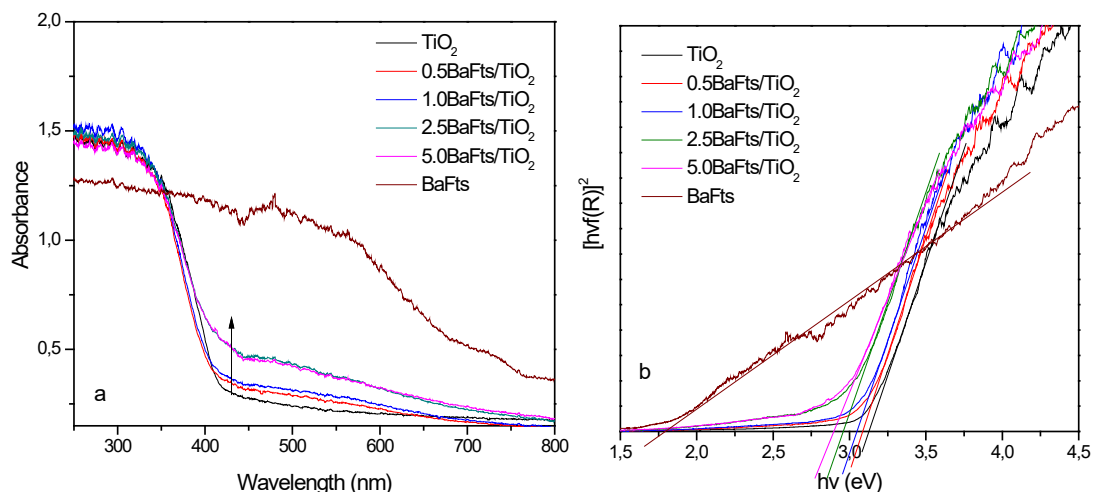


Figure 2. UV-vis absorption spectra of the photocatalysts (a); Band gap energy calculation curves of the photocatalysts (b)

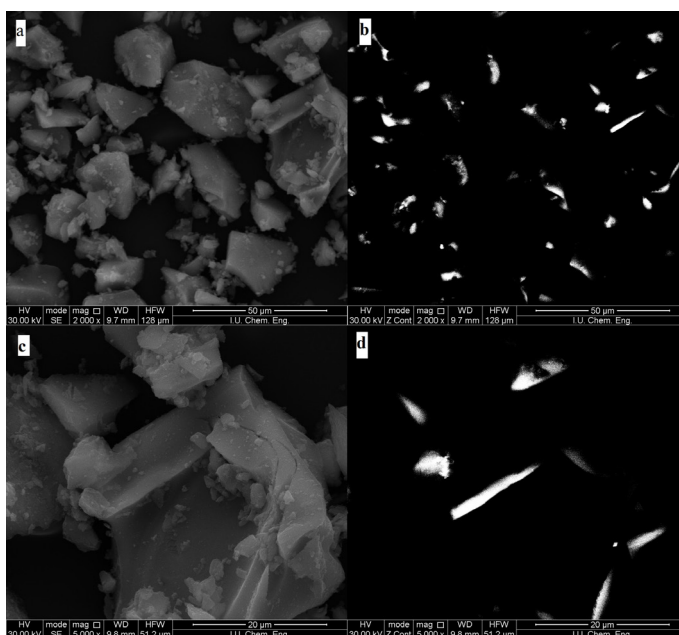


Figure 3. SEM images of the photocatalysts (a, c), SEM images of back scattered electron analysis of the photocatalysts (b, d).

range (>400 nm). The visible light absorbance of the photocatalysts increased as the molar ratio of BaFts increases. The direct band gap energy of the samples was calculated by using the formula in Equation 3 where E_g is the band gap energy, h is Planck’s constant, ν is the frequency of vibration, $h\nu$ is the photon energy, A is a proportional constant and α is the absorption coefficient.

$$(h\nu \pm)^{1/n} = A(h\nu - E_g) \quad (3)$$

The absorbance or Kubelka-Munk function of the reflectance ($f(R)$) is proportional to the absorption coefficient, a . [30,31]. $n=1/2$ is used assuming the direct allowed transitions. A plot of $(hf(R))^2$ versus photon energy, $h\nu$ (Figure 2b) was given for all the photocatalysts explained by the Tauc method [32-34]. The calculated band gap

energies of the prepared photocatalyst samples were given in Table 1. In agreement with the high absorbance in visible range BaFts has 1.80 eV band gap energy, and with the addition of it to TiO_2 the band gap energy decreases.

Figure 3 represents the SEM images of 1.0 BaFts/ TiO_2 in different magnifications. Figure 3b and 3d shows the back scattered electron analysis images of Figure 3a and 3c, respectively. Back scattered electron analysis was performed to detect the BaFts phases on the sample’s surface topography. The heavy molecule barium ferrites appeared brighter in the images. Thus, it is confirmed that the photocatalyst samples contain homogeneously distributed barium ferrites in the structure.

Table 1. Characterization results of prepared photocatalysts.

Photocatalyst	Phase	Diffraction Angle (°)	Crystallite size (nm)	Band gap (eV)
TiO_2	Anatase	25.4	19.2	3.09
0.5 BaFts/ TiO_2	Anatase	25.3	14.3	3.05
1.0 BaFts/ TiO_2	Anatase	25.3	12.8	3.03
2.5 BaFts/ TiO_2	Anatase	25.4	12.8	2.98
5.0 BaFts/ TiO_2	Anatase	25.4	12.8	2.95
Barium ferrites	$BaFe_{12}O_{19}$, $BaFe_2O_4$	34.1	39.2	1.80

Photocatalytic Activity of BaFts/TiO₂ samples

Figure 4 shows the degradation results corresponding to every thirtieth minute during the reaction time. The naked TiO₂ showed the lowest activity. This is attributed to a wide band gap of TiO₂, thus limited activation occurs by visible light. When barium ferrites were added to TiO₂, the activity for degradation of Rhodamine B was increased. The optimum barium ferrite ratio was identified for maximum degradation; at the end of the 4 h reaction time, 69% degradation was achieved by 1.0 BaFts/TiO₂ as seen in Figure 4 and Table 1. Band gap of 1.0 BaFts/TiO₂ was calculated as 3.03 eV, 0.5 BaFts/TiO₂ was 3.05 eV and the naked TiO₂ was 3.09 eV. Namely, as barium ferrite's amount increases in the photocatalyst structure, band gap decreases and activity under visible light increases. But, this situation continues to reach the optimum amount of the barium ferrites. It is reported, when barium ferrite amount was increased from 1.0 to 2.5, the degradation decreased from 69% to 59%. Even 5.0 BaFts/TiO₂ showed 44% conversion despite its lowest band gap (2.95 eV). The optimum addition amount of barium ferrites was found as 1.0% (w/w) barium ferrites/photocatalyst.

As a result of the previous experimental set, 1.0 BaFts/TiO₂ achieved the highest activity. So this sample was used in all other experiments to obtain optimum reaction conditions. Figure 5 shows the degradation efficiency, according to the different photocatalyst loadings. An increase was observed in the degradation efficiency when the photocatalyst dosage was increased from 0.5 g/L to 1.5 g/L. The degradation efficiencies were 51% and 84% for 0.5 g/L to 1.5 g/L, respectively. When

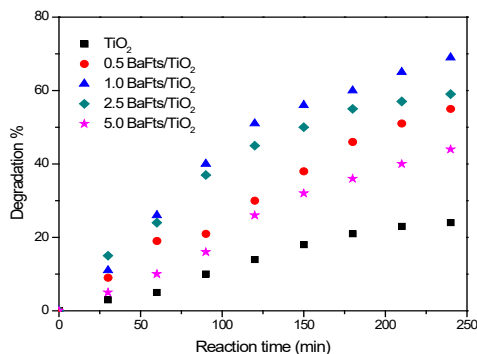


Figure 4. Rhodamine B degradation results under visible light (main wavelength 530 nm).

the photocatalyst dosage was increased to 2.0 g/L, the degradation efficiency decreased to 55%. This situation was attributed to surface area loss due to agglomeration. High photocatalyst loading caused agglomeration and the photocatalyst surface became unavailable for photon absorption [4].

Different initial concentrations (5-20 ppm) were studied. Figure 6 shows the degradation % values versus irradiation time with different initial rhodamine B concentrations. An inverse relation was observed between the initial dye concentration and the degradation efficiency. As the initial dye concentration increased, the degradation efficiency decreased. This result is attributed to the lower adsorption of dye at higher initial concentrations. Thus, the remaining dissolved dye (unadsorbed) hindered the photocatalyst to absorb the photon [1,35]. The maximum degradation was achieved with 5 ppm initial dye degradation using 1 g/L 1.0 BaFts/TiO₂; the value is 93.5%.

It is important to examine the pH effect on photocatalytic reactions because pH is a determining factor to complete removal of the dye. That is related to ionization state of both the catalyst surface and reactant [36]. Figure 7 shows the degradation % values versus the initial pH of the rhodamine B solutions. pH (2.5, 4.5, 6.5, 9.5) effect on the photocatalytic degradation of rhodamine B (10 ppm) was studied under visible light with 1 g/L 1.0 BaFts/TiO₂ photocatalyst. The maximum degradation efficiency was achieved at pH 2.5 (83.5%). Among the range of pH 2.5-9.5 the degradation efficiency decreased with the pH. TiO₂ surface charges are related to pH as follows; if

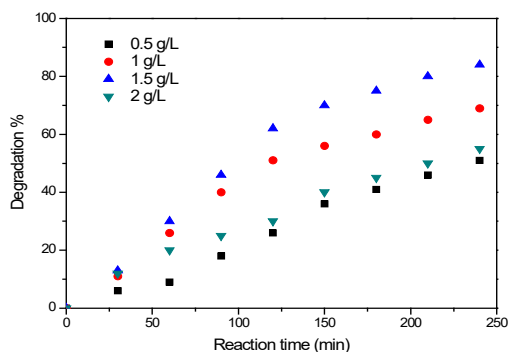


Figure 5. The effect of the photocatalyst dosage on the Rhodamine B degradation under visible light.

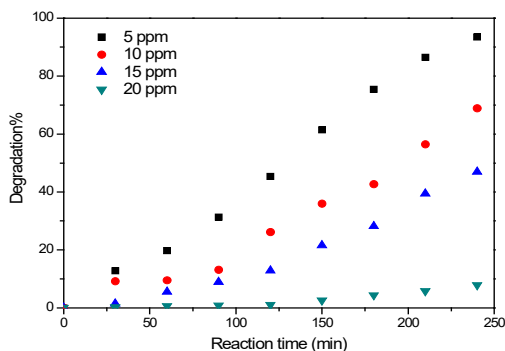


Figure 6. The effect of the initial concentration on the Rhodamine B degradation under visible light.

$pH < pH_{pzc}$, the surface is positively charged $TiOH + H = TiOH_2^+$; if $pH > pH_{pzc}$ surface is negatively charged $TiOH + OH^- = TiO^- + H_2O$ [35-37]. The reported point of zero charge for TiO_2 is 6.4 [36]. Also ionization state of dye molecule is related to pH; rhodamine B has three positively charged forms: if $pH < 1$ it is RBH_2^{2+} , if $pH = 1-3$ it is RB^+ , if $pH > 4$ it is Rb^\pm [38]. In this study, pH effect on photodegradation of rhodamine B can not explain with the electrostatic attraction or repulsion forces between the surface and the rhodamine B ions. Because at pH 2.5, the surface is positively charged ($TiOH_2^+$) and rhodamine B is in cationic form (RB^+). The adsorption is expected to be weak in comparison with higher pH because of repulsion forces of the same charges. However, the maximum degradation was achieved at pH 2.5, this was attributed to the monomeric form of rhodamine B molecules at this pH. When $pH > 4$ the zwitterionic form of rhodamine B molecules are tended to aggregate. The result of aggregation of rhodamine B molecules is the bigger molecular form (dimer) and they are unable to enter the pore of the photocatalyst [39]. That is why the decrease

occurred by the pH increases.

Kinetics

Langmuir-Hinshelwood rate expression has been fitted well with the relationship between the initial degradation rate and the concentration of the organic dye for heterogeneous photocatalytic processes occurring at the solid-liquid interface [40,41]. Langmuir-Hinshelwood kinetic model was given as:

$$r = -\frac{dC_e}{dt} = \frac{k \cdot K \cdot C_e}{1 + K \cdot C_e} \tag{4}$$

where r is the initial disappearance rate of the dye, C_e is the equilibrium dye concentration, t is the time of the reaction, K is the equilibrium constant for the adsorption of the organic dye onto the catalyst, and k is the reaction rate constant. When the dye concentration is very low, $K \cdot C_e$ is very small compared to 1; the term $K \cdot C_e$ is negligible. The equation was integrated with respect to t , so it can be expressed as a pseudo-first-order kinetic equation. The term $k \cdot K$ was used as k_{app} in Equation 5.

$$-\ln \frac{C_e}{C_0} = k_{app} \cdot t \tag{5}$$

Apparent first-order rate constants (k_{app}), and corresponding correlation coefficients (R^2) are summarized in Table 2. The maximum reaction rate constant was found as $9.1 \times 10^{-3} \text{ min}^{-1}$ for 1.0 BaFts/ TiO_2 with 1 g/L loading and 5 ppm initial dye concentration.

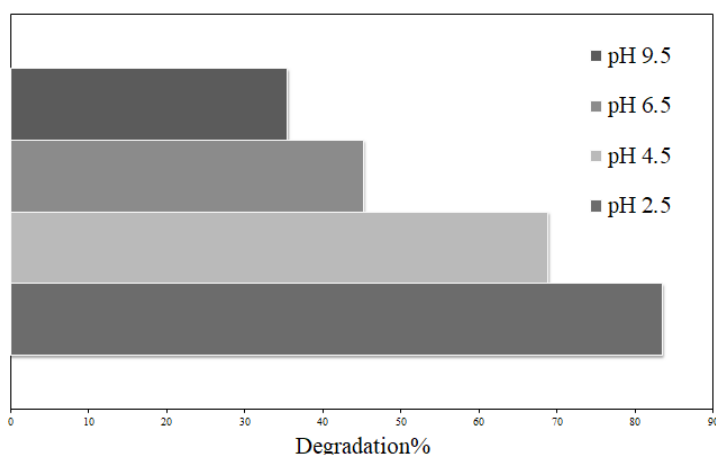


Figure 7. pH Effect on the Rhodamine B degradation under visible light.

Table 2. Rhodamine B degradation reaction conditions and corresponding result.

Photocatalyst	Initial dye	Photocatalyst loading (g/L)	pH	Degradation %	Reaction Rate Constant (min ⁻¹)	R ²
TiO ₂	10	1	4.5	24.8	0.0012	0.98
0.5 BaFts/TiO ₂	10	1	4.5	55.0	0.0033	0.99
1.0 BaFts/TiO ₂	10	1	4.5	68.8	0.0051	0.99
2.5 BaFts/TiO ₂	10	1	4.5	59.0	0.0042	0.95
5.0 BaFts/TiO ₂	10	1	4.5	44.0	0.0024	0.99
1.0 BaFts/TiO ₂	5	1	4.5	93.5	0.0091	0.88
1.0 BaFts/TiO ₂	15	1	4.5	47.0	0.0021	0.85
1.0 BaFts/TiO ₂	20	1	4.5	7.9	0.0003	0.83
1.0 BaFts/TiO ₂	10	0.5	4.5	51.0	0.0029	0.98
1.0 BaFts/TiO ₂	10	1.5	4.5	84.0	0.0077	0.99
1.0 BaFts/TiO ₂	10	2	4.5	55.0	0.0033	0.99
1.0 BaFts/TiO ₂	10	1	2.5	83.5	0.0061	0.89
1.0 BaFts/TiO ₂	10	1	6.5	45.2	0.0026	0.97
1.0 BaFts/TiO ₂	10	1	9.5	35.5	0.0017	0.95

CONCLUSION

This work demonstrates synthesis of barium ferrites loaded TiO₂ nanoparticles by a simple two-step method and their usage in photocatalytic processes. The photocatalytic properties were enhanced by the modification and the optimum amount of BaFts was determined. Maximum degradation efficiency was obtained as 93.5% with 5 ppm initial dye degradation using 1 g/L 1.0 BaFts/TiO₂.

References

- S. Kaur, V. Singh, TiO₂ mediated photocatalytic degradation studies of Reactive Red 198 by UV irradiation, *J. Hazard. Mater.*, 141 (2007) 230-236.
- B. Lee, W. Liaw, J. Lou, Photocatalytic decolorization of methylene blue in aqueous TiO₂ suspension, *Environ. Eng. Sci.*, 16 (1999) 165-175.
- A.N. Ökte, S. Akalin, Iron (Fe³⁺) loaded TiO₂ nanocatalysts: characterization and photoreactivity, *React. Kinet. Mech. Cat.*, 100 (2010) 55-70.
- U.G. Akpan, B.H. Hameed, Parameters affecting the photocatalytic degradation of dyes using TiO₂-based photocatalysts: A review, *J. Hazard. Mater.*, 170 (2009) 520-529.
- H. Park, Y. Park, W. Kim, W. Choi, Surface modification of TiO₂ photocatalyst for environmental applications, *J. Photoch. Photobio. C*, 15 (2013) 1-20.
- A. Galinska, J. Walendziewski, Photocatalytic water splitting over Pt-TiO₂ in the presence of sacrificial reagents, *Energ. Fuel.*, 19 (2005) 1143-1147.
- H. Zhang, C. Liang, J. Liu, Z. Tian, G. Wang, W. Cai, Defect-mediated formation of Ag cluster-doped TiO₂ nanoparticles for efficient photodegradation of pentachlorophenol, *Langmuir*, 28 (2012) 3938-3944.
- B. Liu, X. Wang, G. Cai, L. Wen, Y. Song, X. Zhao, Low temperature fabrication of V-doped TiO₂ nanoparticles, structure and photocatalytic studies, *J. Hazard. Mater.*, 169 (2009) 1112-1118.
- D.R. Baker, P.V. Kamat, Photosensitization of TiO₂ nanostructures with CdS quantum dots: Particulate versus tubular support architectures, *Adv. Funct. Mater.*, 19 (2009) 805-811.
- Y.C. Nah, A. Ghicov, D. Kim, S. Berger, P. Schmuki, TiO₂-WO₃ Composite Nanotubes by Alloy Anodization: Growth and Enhanced Electrochromic Properties, *J. Am. Chem. Soc.*, 130 (2008) 16154-16155.
- E. Casbeer, V.K. Sharma, X.Z. Li, Synthesis and photocatalytic activity of ferrites under visible light: a review, *Sep. Purif. Technol.*, 87 (2012) 1-14.
- S.D. Jadhav, P.P. Hankare, R.P. Patil, R. Sasikala, Effect of sintering on photocatalytic degradation of methyl orange using zinc ferrite, *Mater. Lett.*, 65 (2011) 371-373.
- S.W. Cao, Y.J. Zhu, G.F. Cheng, Y.H. Huang, ZnFe₂O₄ nanoparticles: Microwave-hydrothermal ionic liquid synthesis and photocatalytic property over phenol, *J. Hazard. Mater.*, 171 (2009) 431-435.
- M. Su, C. He, V.K. Sharma, M.A. Asi, D. Xia, X. Li, H. Deng, Y. Xiong, Mesoporous zinc ferrite: Synthesis, characterization, and photocatalytic activity with H₂O₂/visible light, *J. Hazard. Mater.*, 211-212 (2012) 95-103.

15. H. Yang, J. Yan, Z. Lu, X. Cheng, Y. Tang, Photocatalytic activity evaluation of tetragonal CuFe_2O_4 nanoparticles for the H_2 evolution under visible light irradiation, *J. Alloy. Compd.*, 476 (2009) 715-719.
16. Z. Zhu, X. Li, Q. Zhao, Y. Li, C. Sun, Y. Cao, Photocatalytic performances and activities of Ag-doped CuFe_2O_4 nanoparticles, *Mater. Res. Bull.*, 48 (2013) 2927-2932.
17. G. Rekhila, Y. Bessekhouad, M. Trari, Visible light hydrogen production on the novel ferrite NiFe_2O_4 , *Int. J. Hydrogen Energ.*, 38 (2013) 6335-6343.
18. P. Guo, G. Zhang, J. Yu, H. Li, X.S. Zhao, Controlled synthesis, magnetic and photocatalytic properties of hollow spheres and colloidal nanocrystal clusters of manganese ferrite, *Colloid. Surface. A*, 395 (2012) 168-174.
19. P. Sathishkumar, R.V. Mangalaraja, S. Anandan, M. Ashokkumar, $\text{CoFe}_2\text{O}_4/\text{TiO}_2$ nanocatalysts for the photocatalytic degradation of reactive red 120 in aqueous solutions in the presence and absence of electron acceptors, *Chem. Eng. J.*, 220 (2013) 302-310.
20. P. Sathishkumar, N. Pugazhenthiran, R.V. Mangalaraja, A.M. Asiri, S. Anandan, ZnO supported CoFe_2O_4 nanophotocatalysts for the mineralization of direct blue 71 in aqueous environments, *J. Hazard. Mater.*, 252-253 (2013) 171-179.
21. Y. Hou, X. Li, Q. Zhao, G. Chen, ZnFe_2O_4 multi-porous microbricks/graphene hybrid photocatalyst: facile synthesis, improved activity and photocatalytic mechanism, *Appl. Catal. B Environ.*, 142-143 (2013) 80-88.
22. L. Sun, R. Shao, L. Tang, Z. Chen, Synthesis of $\text{ZnFe}_2\text{O}_4/\text{ZnO}$ nanocomposites immobilized on graphene with enhanced photocatalytic activity under solar light irradiation, *J. Alloy. Compd.*, 564 (2013) 55-62.
23. R. Dom, R. Subasri, K. Radha, P.H. Borse, Synthesis of solar active nanocrystalline ferrite, MFe_2O_4 (M: Ca, Zn, Mg) photocatalyst by microwave irradiation, *Solid State Commun.*, 151 (2011) 470-473.
24. L. Zhang, Y. He, Y. Wu, T. Wu, Photocatalytic degradation of RhB over $\text{MgFe}_2\text{O}_4/\text{TiO}_2$ composite materials, *Mater. Sci. Eng. B Adv.*, 176 (2011) 1497-1504.
25. Y. Yang, Y. Jiang, Y. Wang, Y. Sun, L. Liu, J. Zhang, Influences of sintering atmosphere on the formation and photocatalytic property of BaFe_2O_4 , *Mater. Chem. Phys.*, 105 (2007) 154-156.
26. S. Lee, J. Drwiega, D. Mazyck, C.Y. Wu, W. M. Sigmund, Synthesis and characterization of hard magnetic composite photocatalyst-Barium ferrite/silica/titania, *Mater. Chem. Phys.*, 96 (2006) 483-488.
27. C. Valero-Luna, S.A. Palomares-Sanchéz, F. Ruíz, Catalytic activity of the barium hexaferrite with H_2O_2 /visible light irradiation for degradation of methylene blue, *Catal. Today*, 266 (2016) 110-119.
28. R.A. Candeia, M.A.F. Souza, M.I.B. Bernardi, S.C. Maestrelli, I.M.G. Santos, A.G. Souza, E. Longo, Monoferrite BaFe_2O_4 applied as ceramic pigment, *Ceram. Int.*, 33 (2007) 521-525.
29. R. Babuta, I. Lazau, C. Pacurariu, R.I. Lazau, Barium hexaferrite synthesis via the citrate method, *Chem. Bull. "POLITEHNICA" Univ. (Timisoara)*, 59 (2014) 31-35.
30. N. Kislov, S.S. Srinivasan, Y. Emirov, E.K. Stefanakos, Optical absorption red and blue shifts in ZnFe_2O_4 nanoparticle, *Mater. Sci. Eng. B Adv.*, 153 (2008) 70-77.
31. F. Yakuphanoğlu, Electrical characterization and device characterization of ZnO microring shaped films by sol-gel method, *J. Alloy. Compd.*, 507 (2010) 184-189.
32. M. Asiltürk, F. Sayılkan, E. Arpaç, Effect of Fe^{3+} ion doping to TiO_2 on the photocatalytic degradation of malachite green dye under UV and vis-irradiation, *J. Photoch. Photobiol. A*, 203 (2009) 64-71.
33. W. Septina, S. Ikeda, M.A. Khan, T. Hirai, T. Harada, M. Matsumura, L.M. Peter, Potentiostatic electrodeposition of cuprous oxide thin films for photovoltaic applications, *Electrochim. Acta*, 56 (2011) 4882-4888.
34. N. Singh, R.M. Mehra, A. Kapoor, Synthesis and characterization of ZnO nanoparticles, *J. Nano-Electron. Phys.*, 3 (2011) 132-139.
35. Ö. Kerkez, İ. Boz, Photodegradation of methylene blue with $\text{Ag}_2\text{O}/\text{TiO}_2$ under visible Light: operational parameters, *Chem. Eng. Commun.*, 202 (2015) 534-541.
36. D. Maruthamani, D. Divakar, M. Kumaravel, Enhanced photocatalytic activity of TiO_2 by reduced graphene oxide in mineralization of rhodamine B dye, *J. Ind. Eng. Chem.*, 30 (2015) 33-43.
37. R. Vargas, O. Núñez, Hydrogen bond interactions at the TiO_2 surface: Their contribution to the pH dependent photo-catalytic degradation of p-nitrophenol, *J. Mol. Catal. A Chem.*, 300 (2009) 65-71.
38. M.F. Hou, C.X. Mac, W.D. Zhang, X.Y. Tang, Y.N. Fan, H.F. Wan, Removal of rhodamine B using iron-pillared bentonite, *J. Hazard. Mater.*, 186 (2011) 1118-1123.
39. Y. Guo, J. Zhao, H. Zhang, S. Yang, J. Qi, Z. Wang, H. Xu, Use of rice husk-based porous carbon for adsorption of rhodamine B from aqueous solutions, *Dyes Pigments*, 66 (2005) 123-128.
40. K. Naeem, F. Ouyang, Preparation of Fe^{3+} -doped TiO_2 nanoparticles and its photocatalytic activity under UV light, *Physica B*, 405 (2010) 221-226.
41. Y.H. Xu, D.H. Liang, M.L. Liu, D.Z. Liu, Preparation and characterization of $\text{Cu}_2\text{O}-\text{TiO}_2$: Efficient photocatalytic degradation of methylene blue, *Mater. Res. Bull.*, 43 (2008) 3474-3482.

